The Journal of Chemical Physics ARTICLE scitation.org/journal/jcp

Machine learning interatomic potential developed for molecular simulations on thermal properties of β-Ga_2O_3

Cite as: J. Chem. Phys. 153, 144501 (2020); doi: 10.1063/5.0027643
Submitted: 30 August 2020 • Accepted: 22 September 2020 •
Published Online: 8 October 2020

Yuan-Bin Liu,[1] Jia-Yue Yang,[2,3,a)] Gong-Ming Xin,[2] Lin-Hua Liu,[2,3] Gábor Csányi,[4] and Bing-Yang Cao[1,b)]

AFFILIATIONS

[1]Key Laboratory for Thermal Science and Power Engineering of Ministry of Education, Department of Engineering Mechanics, Tsinghua University, Beijing 100084, China
[2]School of Energy and Power Engineering, Shandong University, Jinan, Shandong 250061, China
[3]Optics and Thermal Radiation Research Center, Shandong University, Qingdao, Shandong 266237, China
[4]Engineering Laboratory, University of Cambridge, Trumpington Street, Cambridge CB2 1PZ, United Kingdom

[a)]jy_yang@sdu.edu.cn
[b)]**Author to whom correspondence should be addressed:** caoby@tsinghua.edu.cn

ABSTRACT

The thermal properties of β-Ga_2O_3 can significantly affect the performance and reliability of high-power electronic devices. To date, due to the absence of a reliable interatomic potential, first-principles calculations based on density functional theory (DFT) have been routinely used to probe the thermal properties of β-Ga_2O_3. DFT calculations can only tackle small-scale systems due to the huge computational cost, while the thermal transport processes are usually associated with large time and length scales. In this work, we develop a machine learning based Gaussian approximation potential (GAP) for accurately describing the lattice dynamics of perfect crystalline β-Ga_2O_3 and accelerating atomic-scale simulations. The GAP model shows excellent convergence, which can faithfully reproduce the DFT potential energy surface at a training data size of 32 000 local atomic environments. The GAP model is then used to predict ground-state lattice parameters, coefficients of thermal expansion, heat capacity, phonon dispersions at 0 K, and anisotropic thermal conductivity of β-Ga_2O_3, which are all in excellent agreement with either the DFT results or experiments. The accurate predictions of phonon dispersions and thermal conductivities demonstrate that the GAP model can well describe the harmonic and anharmonic interactions of phonons. Additionally, the successful application of our GAP model to the phonon density of states of a 2500-atom β-Ga_2O_3 structure at elevated temperature indicates the strength of machine learning potentials to tackle large-scale atomic systems in long molecular simulations, which would be almost impossible to generate with DFT-based molecular simulations at present.

I. INTRODUCTION

As a promising semiconductor material, beta-phase gallium oxide (β-Ga_2O_3) exhibits ultrawide bandgap, large electrical breakdown strength, and excellent thermal stability.[1,2] The bandgap of β-Ga_2O_3 is up to ~4.8 eV,[3] which is even larger than that of GaN (~3.4 eV).[4,5] Moreover, the unique properties endow β-Ga_2O_3 with a higher breakdown voltage and higher breakdown field than GaN.[4] This results in the Baliga's figure of merit of β-Ga_2O_3 approaching four times larger than that of GaN. In addition to the lower production cost of bulk β-Ga_2O_3 crystals than that of GaN,[6,7] β-Ga_2O_3, thus, has been treated as an ideal candidate for the next-generation high-power, high-frequency, and high-efficiency electronic devices.

Besides these excellent electronic properties, the thermal properties of β-Ga_2O_3 are evidently critical for its application in

high-power devices.[8,9] High heat dissipation in a β-Ga_2O_3-based device can cause excessive temperature driven by self-heating, resulting from the relatively low thermal conductivity of β-Ga_2O_3, which is one order of magnitude lower than that of GaN (~240 W m^{-1} K^{-1} at room temperature).[10–12] The increase in the electron–phonon scattering at high temperature will degrade the electron transport, resulting in the loss of performance of the β-Ga_2O_3-based devices. Therefore, a thorough knowledge of the thermal properties of β-Ga_2O_3 is fundamental and significant for facilitating the development of effective thermal management strategies to advance the high-power devices based on β-Ga_2O_3.

Atomic-scale simulations have long been a central approach to provide the deep insight into the thermal properties of β-Ga_2O_3. There are two routine atomic-scale modeling techniques, i.e., explicit quantum chemical methods mostly based on density functional theory (DFT) and molecular dynamics (MD) simulations using simple empirical potentials. State-of-the-art DFT methods that treat electron explicitly can accurately sample the potential energy surface (PES) of a set of atoms and atomic forces from the partial derivatives of the total energy. However, considering large time and length scales of thermal transport processes, high computational cost limits the DFT methods for modeling thermal transport properties. Simple empirical potentials with certain functional forms are several orders of magnitude faster than DFT.[13,14] Nevertheless, the parameters in empirical potentials are usually optimized by fitting specific physical properties, which makes empirical potentials less accurate and less transferrable than DFT to other physical properties not employed to optimize parameters.[15] The Buckingham potential is a typical empirical potential for β-Ga_2O_3. There are two available studies reporting the potential for β-Ga_2O_3,[16,17] while both of them generate remarkably distinct phonon dispersions from DFT. When it comes to the thermal conductivity prediction, the anharmonic interactions of phonons have to be well described, which places a greater demand on the accuracy of interatomic potentials.

Recently, a methodology generating interatomic potentials by machine learning (ML) is beginning to emerge, which has shown great potential for getting rid of the aforementioned trade-off between cost and accuracy.[13] The core of the ML potentials is a representation of the PES through a set of local environment descriptors. After obtaining the adequate sampled data of the PES on the desired regions of phase space by quantum-mechanical calculations, the ML algorithms are used to accurately interpolate energies and forces for arbitrary structures. Unlike the empirical potentials, the ML potentials do not require a prior assumption about the functional form. The mappings between the PES and the local environment descriptors can be directly learned from the reference data, which makes the ML potentials an unbiased representation of the PES and resultantly possess good transferability.[18,19] So far, there are several successfully developed ML potentials, such as the neural network potential,[20,21] the Gaussian approximation potential (GAP),[18,22] the spectral neighbor analysis potential,[23,24] the moment tensor potential,[25,26] the atomic cluster expansion potential,[27] and the atomic permutationally invariant polynomials potential.[28] It has been confirmed that a well-trained ML potential can give access to atomistic simulations achieving near-DFT accuracy but much cheaper and orders of magnitude faster than the DFT calculations.

In this work, we introduce an accurate interatomic Gaussian approximation potential (GAP) for the single-crystalline β-Ga_2O_3, with the aim of facilitating the effective prediction for its thermal properties from molecular simulations. In Sec. II, we briefly introduce the GAP methodology and illustrate how the configurations of the single-crystalline β-Ga_2O_3 and accurate quantum-mechanical training data are generated. In Sec. III, we first evaluate the maximum accuracy that any finite-range interatomic potential for β-Ga_2O_3 can achieve as a function of its neighbor cutoff. This process is independent of any ML-based potential models. Then, we test how much the accuracy of our GAP model deviates from the maximum accuracy. Finally, we present the results of the ground-state lattice parameters, heat capacity, coefficients of thermal expansion (CTE), phonon dispersions at 0 K, and anisotropic thermal conductivity of β-Ga_2O_3 as predicted by our GAP model. Furthermore, we compare the calculation results with the DFT benchmarks and some experimental data to assess the performance of the potential. Finally, our GAP model is applied to generate the phonon density of states (PDOSs) of a large-scale β-Ga_2O_3 structure at finite temperature. Main conclusions of this study are summarized in Sec. IV.

II. METHODOLOGY

A. Construction of a Gaussian approximation potential

Herein, we outline the general procedure of how a Gaussian approximation potential is constructed. There are three ingredients to achieve this goal.

The first ingredient is to sample a set of reference configurations on the desired regions of phase space and associated quantum-mechanical data including accurate total energies, forces on atoms, and virial stresses. These original reference data are then stored according to a suitable database format for training and testing.

The second ingredient is to convert the atomic configurations to the suitable machine-readable data as inputs for the PES fit. As fundamental symmetry requirements, all descriptors for atomic environment have to be invariant to translation, rotation, and permutation with respect to atom indexing. For the β-Ga_2O_3 crystals, the many-body interactions should be taken into consideration to guarantee the accuracy of potentials. A many-body descriptor can comprise the information of all neighbors of a centered atom up to a given cutoff radius. This work adopts the so-called "Smooth Overlap of Atomic Position" (SOAP) descriptor, which is initially developed for use with GAP.[22] Although the SOAP representation is not strictly complete along with many similar two- and three-body representations,[29] it is a widely used general atom-centered representation[30–32] and is the basis of many successful ML potentials.[33–42]

The final ingredient is to complete the PES fit based on the ML approaches mapping reference energies from descriptors. GAP adopts a kernel-based ML method, i.e., Gaussian process regression,[43] to carry out the fit. In the practical implementation of GAP, the total energy of the system is decomposed into individual atomic contributions,

$$E = \sum_i \varepsilon(\mathbf{q}_i), \tag{1}$$

where $\varepsilon(\mathbf{q}_i)$ is the energy contribution of the ith atom and $\mathbf{q}_i$ is a descriptor characterizing the local atomic environment around the ith atom. The local atomic energy contribution $\varepsilon(\mathbf{q}_i)$ is given by a linear combination of kernel functions,

$$\varepsilon(\mathbf{q}_i) = \sum_j \alpha_j K(\mathbf{q}_i, \mathbf{q}_j), \tag{2}$$

where K is a fixed kernel function quantifying the degree of similarity between the atomic environments described by $\mathbf{q}_i$ and $\mathbf{q}_j$. Such a "kernel trick" is a common strategy to solve the nonlinear regression problem in ML-based methodologies.[44] The unknown coefficient vector $\boldsymbol{\alpha}$ is determined via the fitting procedure of machine learning. In SOAP, the local environment of the ith atom is represented by its neighbor density function within a given cutoff r_{cut},

$$\rho_i(\mathbf{r}) = \sum_j f_{cut}(r_{ij}) \exp\left[-\frac{(\mathbf{r}_i - \mathbf{r}_{ij})^2}{2\sigma_{at}^2}\right], \tag{3}$$

where $\mathbf{r}_i$ denotes the position vector of atom i and σ_{at} controls the smoothness of the potential. Here, f_{cut} is a cutoff function going smoothly to 0 at r_{cut} and takes the form of

$$f_{cut}(r) = \begin{cases} 1, & r < r_{cut} - \Delta r, \\ \frac{1}{2}\left[1 + \cos\left(\frac{r - r_{cut} + \Delta r}{\Delta r}\pi\right)\right], & r_{cut} - \Delta r < r \le r_{cut}, \\ 0, & r > r_{cut}, \end{cases} \tag{4}$$

where Δr denotes the cutoff transition width in which f_{cut} decreases smoothly from 1 to 0. Atomic neighbor densities are then expanded in a local basis set of orthogonal radial basis functions $g_n(\mathbf{r})$ and spherical harmonics Y_{lm} as

$$\rho_i(\mathbf{r}) = \sum_{n<n_{\max}} \sum_{l<l_{\max}} \sum_{m=-l}^{l} c_{nlm}^i g_n(r) Y_{lm}\left(\frac{\mathbf{r}}{r}\right), \tag{5}$$

where c_{nlm}^i are the expansion coefficients. The spherical power spectrum of these expansion coefficients then forms the descriptor as

$$(\mathbf{q}_i)_{nn'l} = \frac{1}{\sqrt{2l+1}} \sum_m (c_{nlm}^i)^* c_{n'lm}^i, \tag{6}$$

which is strictly translational, rotational, and permutational invariance. For the many-body SOAP descriptor, the dot product kernel is the natural choice, which is determined by

$$K(\mathbf{q}_i, \mathbf{q}_j) = \left|\frac{\mathbf{q}_i \cdot \mathbf{q}_j}{|\mathbf{q}_i| \cdot |\mathbf{q}_j|}\right|^{\zeta}. \tag{7}$$

The role of the positive integer ζ is to improve the sensitivity of the kernel and also increase the body order of the model. To reduce the computational cost, a sparsification method[45] is used for the SOAP kernel. More details about the construction of the Gaussian approximation potential can be found in the literature.[18,22,46] The main hyperparameters used in this work for constructing the descriptors, the kernel functions, and training a GAP are summarized in Table I. The more information about those symbols can be found in the literature.[46,47]

TABLE I. Hyperparameters used in the training of the GAP model.

r_{cut} (Å)	5.5
Δr (Å)	1.0
ζ	4
σ_{at} (Å)	0.5
σ_v^{energy} (eV/atom)	0.0001
σ_v^{force} (eV/Å)	0.01
σ_v^{virial} (eV/atom)	0.01
$n_{\max}$	10
$l_{\max}$	6
Sparse method	CUR
Representative points	5000

B. Generation of training data

The atomic configurations are sampled from various molecular dynamics trajectories using *ab initio* molecular dynamics (AIMD) and MD with various iterations of our GAP model. Once the configurations are determined, the values of the associated energies, forces, and virial stresses are all calculated at the same level of DFT using the Vienna *Ab Initio* Simulation Package (VASP).[48,49] We perform all DFT calculations using the Perdew–Becke–Erzenhof functional[50] with a projector augmented wave method,[51] a plane wave basis cutoff of 520 eV, and a Gaussian smearing of 0.1 eV width. The halting criterion for the self-consistent field iterations is set to 10^{-7} eV. The unit cell of β-Ga_2O_3 with 20 atoms is optimized with a 4 × 16 × 8 grid for Brillouin zone sampling. In the training database, each configuration consists of the 2 × 2 × 2 supercell with 160 atoms. For single point calculations of those supercells in the training database, we have employed a 1 × 4 × 2 **k**-space sampling mesh, which is well-converged with the tolerance in an energy of ~10^{-5} eV/atom and force of ~10^{-4} eV/Å compared with a 2 × 8 × 4 grid.

To describe the thermal transport properties of β-Ga_2O_3, the potential model has to provide precisely harmonic and anharmonic force constants at different volumetric strains. Thus, the GAP model should learn the variation of energies as a function of lattice vectors. To achieve this goal, simulation cells of β-Ga_2O_3 are reconstructed with uniform strains on each lattice constant from −4% to 4% with the step of 1%. In addition to various temperatures to be considered, only using AIMD to generate all trajectories for these simulation cells with different lattice constants will cost a lot of computational sources. To reduce the cost, AIMD is only used to generate the first set of training data for the simulation cell with the fully optimized and relaxed lattice parameters. There are totally 800 snapshots taken with a time step of 40 fs from AIMD at temperatures between 300 K and 1500 K. The total energies, forces, and virial stresses of these atomic configurations are recorded to train the initial GAP model. A further set of trajectories at different volumetric strains are generated using MD with the preliminary GAP model in the NVT ensemble. Single point calculations that are much cheaper than AIMD are then performed to record the total energies, forces, and virial stresses of atomic configurations sampled from MD with a time interval of 445 fs at temperatures between 100 K and 1000 K. The new database comprises of 801 training datasets and 90 testing datasets, which

is used to afresh teach a GAP model. After a few iterations, an improved and accurate GAP model can be obtained in this way. In this work, all training processes are performed using the freely available QUIP package at https://github.com/libAtoms/QUIP.

III. RESULTS AND DISCUSSIONS

For valid implementations of GAP, the assumption about the localization of ε has to hold so that the total energy can be divided into a sum of local terms. Therefore, we will perform locality tests for β-Ga_2O_3. This process, in turn, can determine the maximum accuracy with which any finite-range potential can be approximated. Here, we adopt the similar procedure for carrying out locality tests as employed in the previous literature.[33] We first give an optimized simulation cell of β-Ga_2O_3 with a supercell size of $2 \times 5 \times 3$, comprising 600 atoms. We then consider a central atom and fix all neighbors of the central atom within a sphere of radius r_{fix}. Furthermore, various simulation cells are generated by changing the atomic positions outside the fixed sphere and transferred to DFT to calculate the forces on the central atom. Finally, the locality is characterized by the standard deviation of these forces as a function of r_{fix}.

Figure 1 shows the force locality tests for β-Ga_2O_3 structures, which include two ways of moving atoms. All atomic positions outside r_{fix} are randomly displaced with a standard deviation of 0.1 Å in Fig. 1(a), while large distortions are generated by MD at high temperature in Fig. 1(b). Both Ga and O are chosen as sphere centers for independent locality tests. The results show that the force deviations decay rapidly as r_{fix} increases, and β-Ga_2O_3 exhibits the strong force locality with regard to different distortion ways. We observe that the overall force deviations derived from MD-induced distortions are smaller than those from random distortions. The same phenomenon is also observed in Ref. 33 where a reasonable explanation has been given. Because the training data in this work are generated from MD, the force standard deviations from sample distortions using MD are more suitable to serve as the approximate maximum accuracy that any potential with a certain cutoff radius can achieve. Considering the trade-off between the computational expense during training and the precision requirement, we choose r_{cut} as 5.5 Å to train our GAP model.

After estimating the precision limit of a finite-range potential, we here validate the accuracy of our GAP model based on the DFT reference data. The training and testing datasets contain 384 480 and 43 200 atomistic reference force components, respectively. As shown in Fig. 2, the total energies and atomic forces as predicted by our model are compared with those from DFT. It is observed that the energies are well reproduced by our GAP with a low root-mean-squared error (RMSE) of 0.0003 eV/atom for the testing datasets. Forces in the testing datasets are predicted with an RMSE of 0.050 eV/Å for the Ga atom and 0.038 eV/Å for the O atom, respectively. The results demonstrate that our GAP model is a good representative of *ab initio* PES and, indeed, reaches the target force accuracy, as shown in Fig. 1(b). It is noted that the test error is much higher than the training error for those configurations with higher energy. This can be elucidated by the fact that the intense crystal lattice vibration at elevated temperature leads to an increase in the range of structural parameters, which may affect the extrapolation accuracy of the GAP model. Therefore, sampling more configurations with higher energy to train the GAP may further reduce the test error at elevated temperature. We also perform an investigation for the convergence of the GAPs with the training size. The subsets of 50, 200, 400, and 600 structures are extracted from the total 801 structures to train the GAPs, respectively, with the 90 testing structures being held unchanged. The convergence results with respect to the prediction of energies and forces are shown in Fig. 3. It is observed that the GAP model appears to have simultaneously converged in energy and force at a small training dataset size of ~400 structures. Interestingly, even with a relatively smaller training datasets of ~200 structures, the GAP model also presents a good convergence.

We now move on to evaluate the quality of our GAP for modeling the thermal properties of β-Ga_2O_3. We begin by employing the GAP model to predict the ground-state lattice parameters, which are a fundamental property for any atomistic model and may affect many intrinsic properties of materials. The reproduced lattice parameters by the GAP model are a = 12.51 Å, b = 3.10 Å, and

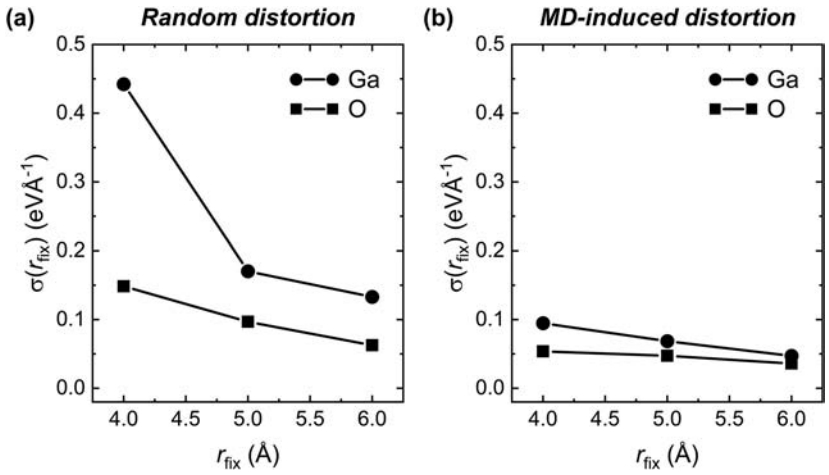

FIG. 1. Force locality tests for β-Ga_2O_3. (a) Structures are created by randomly moving atomic positions outside the fixed sphere. (b) Large structure distortions are generated by MD at high temperature. There are ten independent distortions that are constructed for each central atom.

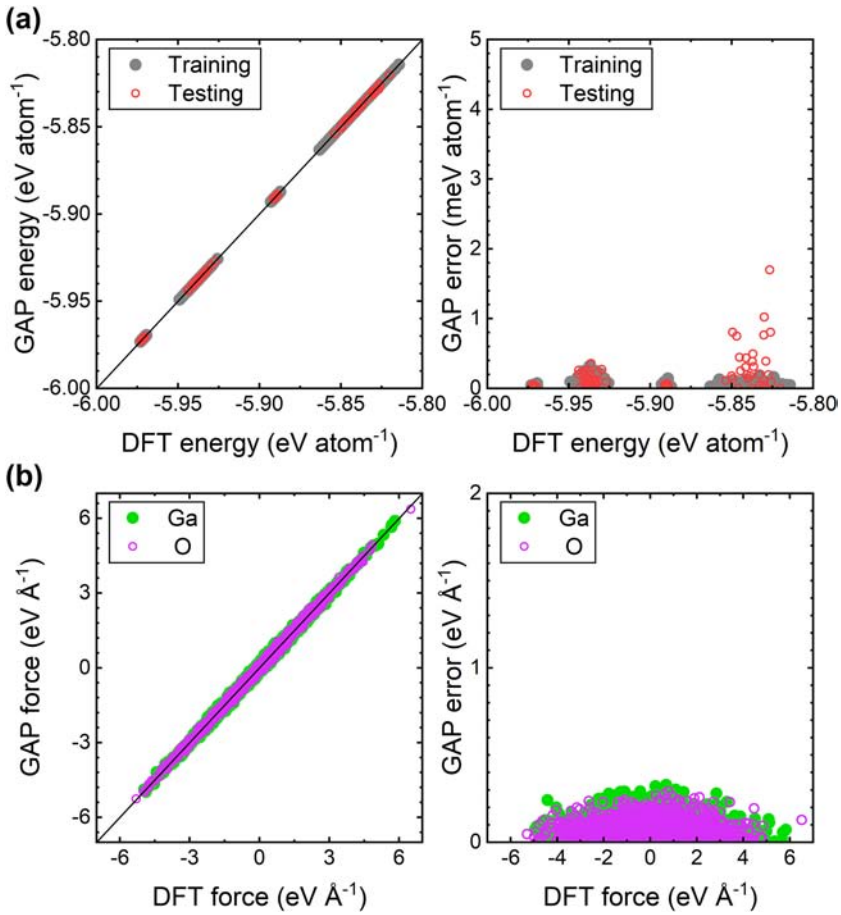

FIG. 2. Comparison of DFT-computed and GAP-predicted (a) total energies and (b) interatomic forces on a test set of 14 400 atomistic environments. Here, error specifically represents the absolute error.

c = 5.92 Å with β = 103.72°, which are in excellent agreement with our DFT results with an error of 0.02%. Moreover, the lattice parameters from our GAP are also in line with the previous computational[7] and experimental results.[52]

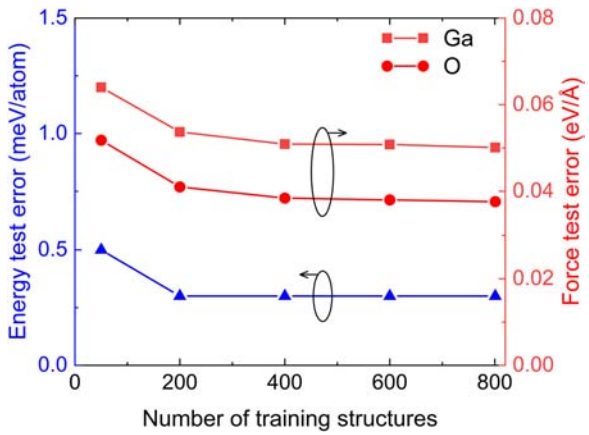

FIG. 3. RMSEs in predicted energies and forces of the testing datasets as a function of the size of the training structures.

Our GAP model is then used to probe the heat capacity and the coefficients of thermal expansion (CTE) of β-Ga_2O_3. The heat capacity is a fundamental and important thermal property. To extract the thermal conductivity values from the time-domain thermoreflectance measurements, it is necessary to know the heat capacity of β-Ga_2O_3 at different temperatures. We calculate the heat capacity of β-Ga_2O_3 under the quasi-harmonic approximation (QHA) using the PHONOPY package.[53] Figure 4(a) summarizes the heat capacity values of β-Ga_2O_3 from our GAP model, the DFT calculations, and the experiment measurements by using a differential scanning calorimeter.[54] It is shown that the data from our GAP model agree well with those from the DFT calculations and the experimental measurements. Recently, the heterostructures integrating β-Ga_2O_3 with other materials emerge to optimize the performance of electronic devices, which has gotten more and more attention.[55–57] In practical applications, the thermal expansion of β-Ga_2O_3 plays a crucial role in determining heteroepitaxial and heterojunction strains caused by thermal mismatch, which contributes to the selection of proper materials for epitaxial growth.[58] Here, the coefficient of thermal expansion of β-Ga_2O_3 is defined as

$$\mathrm{CTE} = \frac{1}{V_T}\frac{\partial V_T}{\partial T}, \tag{8}$$

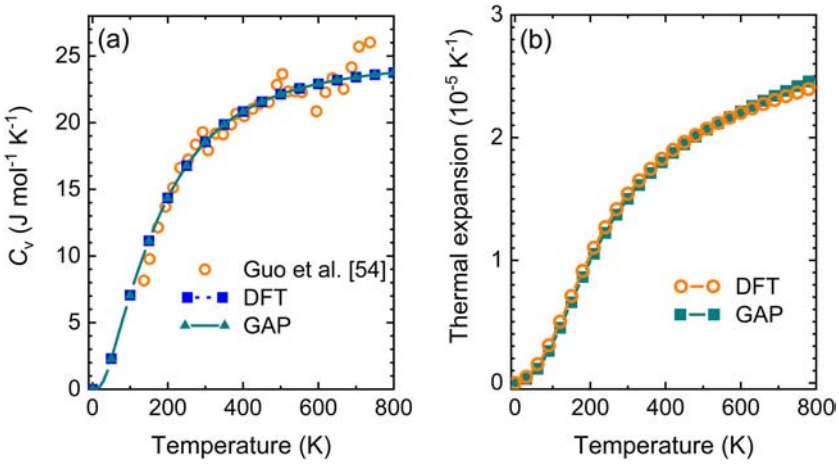

FIG. 4. Temperature-dependent (a) specific heat capacity and (b) thermal expansion coefficients of β-Ga_2O_3.

where V denotes the volume of the β-Ga_2O_3 bulk and T represents the temperature in Kelvin. We calculate the CTEs under the quasi-harmonic approximation using the PHONOPY package.[53] As shown in Fig. 4(b), the GAP model introduced here quantitatively reproduces the thermal expansion determined by DFT calculations. Both GAP and DFT predict that the CTEs are strongly dependent on temperatures between 0 K and 1000 K. It is clear that with an increase in temperature, the CTEs grow rapidly up to ~300 K, and the slopes become smaller at higher temperatures.

The prediction of the phonon dispersions and thermal conductivities of a material is an excellent metric for the quality of a potential to describe the lattice dynamics. We first calculate the second-order harmonic and third-order anharmonic interatomic force constants (IFCs) using the finite displacement method.[59] Combining the PHONOPY package[59] with the second-order IFCs from our GAP and DFT, the phonon dispersions of β-Ga_2O_3 at 0 K are determined, as illustrated in Fig. 5. As a characteristic of the ionic crystal, the splitting of LO–TO phonons at the Γ point is observed,

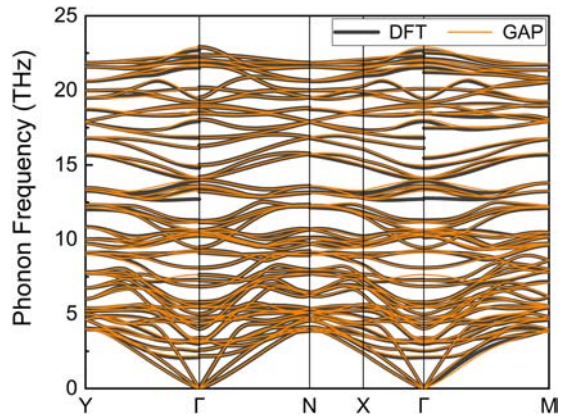

FIG. 5. Phonon dispersion of β-Ga_2O_3 at 0 K predicted by DFT and the GAP model.

which is related to the long-range Coulomb interactions. Because our model is missing the Coulomb interactions, we have added the non-analytical term correction to the dynamical matrix to resolve the splitting of LO–TO phonons at the Γ point. It is shown that the GAP model accurately predicts the phonon frequencies at almost of all high-symmetry points and the dispersion behavior of each phonon branch. As a matter of fact, although the missing Coulomb term leads to some error on the forces, it will be shown that the accuracy of our model is high enough to generate the excellent thermal conductivity. If the long-range Coulomb interactions become important later for other calculations, we can properly put in the Coulomb interaction, with fixed partial charges, and fit the GAP correction on top of that. This will automatically give the correct LO–TO splitting and also improve the accuracy of the forces. Similar treatment for GaN can be found in the literature.[18]

We then use the second-order and third-order IFCs to perform the calculations of the thermal conductivity of β-Ga_2O_3 by solving the phonon Boltzmann transport equation (BTE) using the SHENGBTE package[60] with a 5 × 17 × 9 mesh for sampling the first Brillouin zone over temperatures ranging from 100 K to 600 K. It is expected that the thermal conductivities of β-Ga_2O_3 are anisotropic along the [010], [100], and [001] crystallographic directions due to the monoclinic lattice structure. The thermal conductivity tensor of the monoclinic crystal takes the form of

$$\mathbf{K} = \begin{bmatrix} \kappa_{xx} & 0 & \kappa_{xz} \\ 0 & \kappa_{yy} & 0 \\ \kappa_{xz} & 0 & \kappa_{zz} \end{bmatrix}, \tag{9}$$

where the subscripts x, y, and z correspond to the Cartesian axes. In the construction of the β-Ga_2O_3 supercell, we take [100] and [010] to coincide with the x axis and y axis. At that time, [001] is orthogonal to y axis, and there is an included angle of β between [001] and the x axis. Obviously, the thermal conductivities along the [100] and [010] directions are equal to the components κ_{xx} and κ_{yy}, respectively. However, the thermal conductivity along the [001] direction is calculated from

$$\kappa_{[001]} = \kappa_{xx} \cos^2\beta + \kappa_{xz} \sin 2\beta + \kappa_{zz} \sin^2\beta. \tag{10}$$

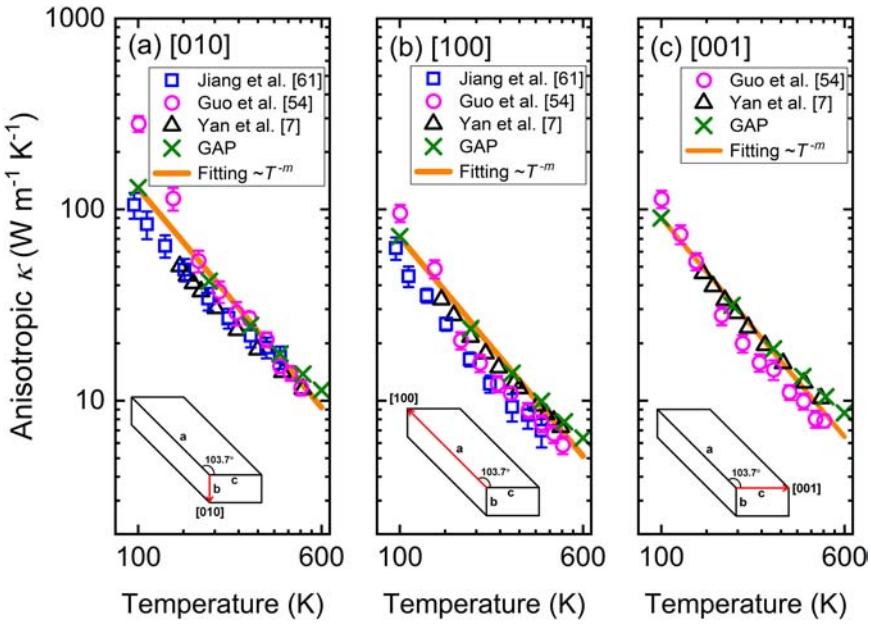

FIG. 6. Comparison of anisotropic thermal conductivity of β-Ga_2O_3 along the (a) [010], (b) [100], and (c) [001] crystallographic directions between the GAP model and the literature results.[7,54,61]

As shown in Fig. 6, the GAP model measures the thermal conductivities of β-Ga_2O_3 along the [010], [100], and [001] crystallographic directions. The thermal conductivity using the GAP shows overall good agreement with the results from DFT[7] and experiments.[54,61] As predicted by GAP, the highest thermal conductivity is along the [010] direction among all three crystallographic directions, while the lowest along [100]. Moreover, the prediction of our GAP shows that the thermal conductivity of β-Ga_2O_3 follows an $\sim 1/T^m$ (m = 1.47) dependence throughout the measured temperature range from 100 K to 600 K. The characteristic of such a relationship indicates that the Umklapp scattering is the dominant phonon scattering mechanism of β-Ga_2O_3.

In Fig. 7, we show more phonon transport characteristics in β-Ga_2O_3, calculated from the GAP model. The accumulated thermal conductivity as a function of the phonon frequency at 300 K is presented in Fig. 7(a). It is clear to see the anisotropy along the three Cartesian axes. Moreover, it is revealed that more than 90% of κ are contributed from low-frequency phonons below 6.5 THz. Figure 7(b) exhibits the phonon relaxation lifetime of β-Ga_2O_3, which is shorter than that of GaN in the almost entire frequency domain.[7] Assuming constant phonon anharmonicity, phonon relaxation lifetime relates linearly to the inverse of the three-phonon scattering phase-space volume. Hence, β-Ga_2O_3 has a larger three-phonon scattering phase space in which there are more channels for supporting three-phonon scattering, resulting in the lower thermal conductivity than GaN.

For a fair comparison between the GAP and DFT results, we have adopted the same supercell with 160 atoms for the calculations of both methods in the above discussion. Not employing a bigger supercell is because of the fact that state-of-the-art DFT methods normally only tackle the system sizes of a few tens or hundreds of atoms. In fact, the MD simulations with GAP can model the system sizes of up to thousands of atoms. Figure 8 shows the total phonon density of states (PDOS) of 2500-atom β-Ga_2O_3 structures

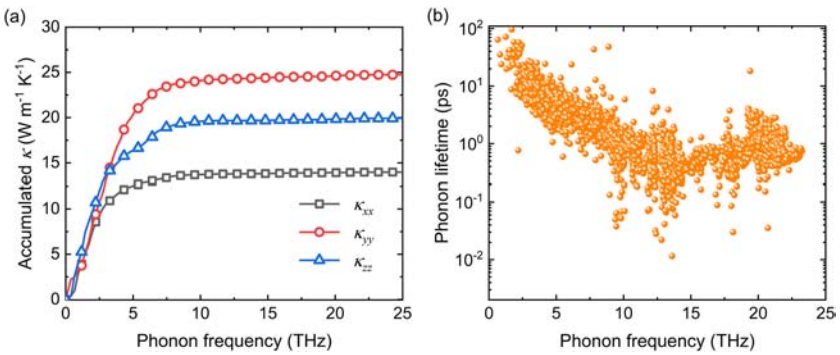

FIG. 7. Analysis of phonon transport in β-Ga_2O_3 by the GAP model. (a) Accumulated thermal conductivity and (b) phonon lifetime as a function of phonon frequency at 300 K.

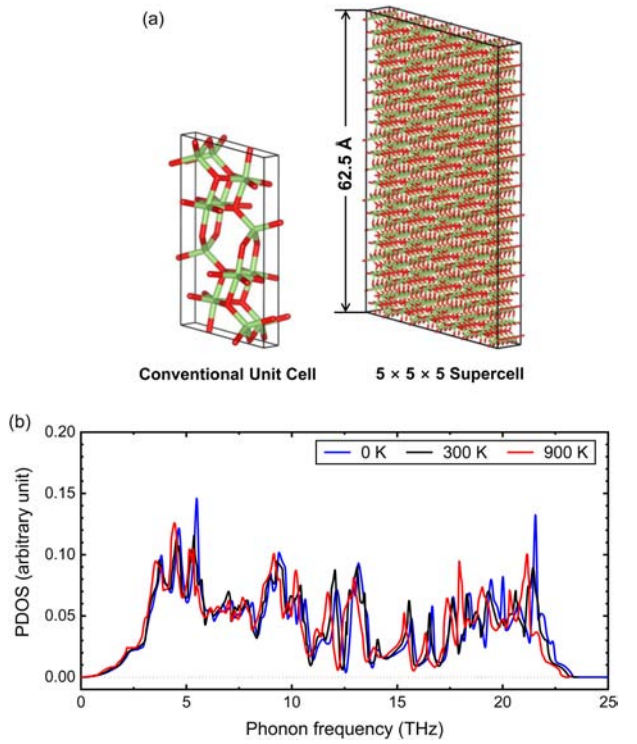

FIG. 8. Large-scale simulations using the GAP: (a) 20-atom and 2500-atom structures of β-Ga_2O_3. Ga atoms are green, and O atoms are red. (b) Phonon density of states of β-Ga_2O_3 at temperatures of 0 K, 300 K, and 900 K.

given by the GAP model at 0 K, 300 K, and 900 K. To calculate the PDOS at 0 K, the finite displacement method has been applied.[59] In order to predict the PDOS at finite temperature, we have employed the normal-mode-decomposition technique to extract anharmonic phonon properties from MD simulations.[62,63] The MD simulations with the GAP model are run in the NVT ensemble. The 2500-atom structure is first equilibrated for 50 ps until the temperature has equilibrated and statistics are collected over 400 ps trajectories. The larger supercell size allows us to more accurately interpolate the quasiparticle phonon frequencies at incommensurate **q**-points. In Fig. 8(b), the phonon density of states $g(\omega)$ is normalized by $\int_0^\infty g(\omega)d\omega = 1$. It is clearly seen that the peaks in the PDOS are redshifted and become wider with an increase in temperature. The temperature-dependent frequency shift is attributed to the coupling between phonons having different momentum and band index. All results from Fig. 8(b) illustrate the capability of GAP to model large-scale atomic systems in long MD simulations. To accomplish the same task, however, the DFT-based simulations are extremely expensive and not feasible.

IV. CONCLUSIONS

In summary, we develop a machine learning based Gaussian approximation potential for atomistic simulations of single-crystalline β-Ga_2O_3. Our GAP model exhibits remarkable accuracy in reproducing the *ab initio* potential energy surface of β-Ga_2O_3, attaining a total energy accuracy of ~0.3 meV/atom and force accuracy below 0.05 eV/Å for both the Ga and O atoms. MD with the GAP model, however, is approximately four orders of magnitude faster than DFT, for 160 atoms. We then employ the GAP model to predict ground-state lattice parameters, heat capacity, coefficients of thermal expansion, phonon dispersions at 0 K, and anisotropic thermal conductivity of β-Ga_2O_3. All these results show excellent agreement with those either from DFT calculations or from experimental measurements. Moreover, it is demonstrated that the GAP can well describe the lattice dynamics of β-Ga_2O_3. Finally, we perform a large-scale simulation using the GAP for the phonon density of states of β-Ga_2O_3 at finite temperature, which demonstrates the capability of GAP to model large-scale atomic systems in long MD simulations. Thus, the GAP models appear to be promising tools to further study the thermal conductivity of β-Ga_2O_3 thin films and interlayer interactions between the substrate and β-Ga_2O_3. Both applications are significant for the development of the high-power devices based on β-Ga_2O_3 but extremely expensive and not even feasible for the DFT-based simulations.

ACKNOWLEDGMENTS

This work was supported by the National Natural Science Foundation of China (Grant Nos. 51825601, 51676108, and 52011530030). J.-Y.Y. is grateful for the support from Shandong University (Qilu Young Scholar Grant No. 89963031), and G.-M.X. acknowledges the support from the Shenzhen Basic Research Program (Grant No. JCYJ20190807092801669).

DATA AVAILABILITY

The training configurations and GAP model files developed herein are freely available in our online repository at http://www.libatoms.org. The data that support the findings of this study are available from the corresponding author upon reasonable request.

REFERENCES

[1]M. Orita, H. Ohta, M. Hirano, and H. Hosono, Appl. Phys. Lett. **77**(25), 4166–4168 (2000).
[2]S. J. Pearton, J. Yang, P. H. Cary IV, F. Ren, J. Kim, M. J. Tadjer, and M. A. Mastro, Appl. Phys. Rev. **5**(1), 011301 (2018).
[3]K. Sasaki, M. Higashiwaki, A. Kuramata, T. Masui, and S. Yamakoshi, J. Cryst. Growth **378**, 591–595 (2013).
[4]K. Sasaki, A. Kuramata, T. Masui, E. G. Víllora, K. Shimamura, and S. Yamakoshi, Appl. Phys. Express **5**(3), 035502 (2012).
[5]D.-S. Tang, G.-Z. Qin, M. Hu, and B.-Y. Cao, J. Appl. Phys. **127**(3), 035102 (2020).
[6]Z. Galazka, K. Irmscher, R. Uecker, R. Bertram, M. Pietsch, A. Kwasniewski, M. Naumann, T. Schulz, R. Schewski, D. Klimm, and M. Bickermann, J. Cryst. Growth **404**, 184–191 (2014).
[7]Z. Yan and S. Kumar, Phys. Chem. Chem. Phys. **20**(46), 29236–29242 (2018).
[8]Y.-C. Hua, H.-L. Li, and B.-Y. Cao, IEEE Trans. Electron Devices **66**(8), 3296–3301 (2019).
[9]M. Yang, M.-T. Li, Y.-C. Hua, W. Wang, and B.-Y. Cao, Int. J. Heat Mass Transfer **160**, 120230 (2020).

[10]Q. Zheng, C. Li, A. Rai, J. H. Leach, D. A. Broido, and D. G. Cahill, Phys. Rev. Mater. **3**(1), 014601 (2019).
[11]Y. Zhang, Q. Su, J. Zhu, S. Koirala, S. J. Koester, and X. Wang, Appl. Phys. Lett. **116**(20), 202101 (2020).
[12]J.-Y. Yang, G. Qin, and M. Hu, Appl. Phys. Lett. **109**(24), 242103 (2016).
[13]V. L. Deringer, M. A. Caro, and G. Csányi, Adv. Mater. **31**(46), 1902765 (2019).
[14]H. Bao, J. Chen, X. Gu, and B. Cao, ES Energy Environ. **1**, 16 (2018).
[15]H. Babaei, R. Guo, A. Hashemi, and S. Lee, Phys. Rev. Mater. **3**(7), 074603 (2019).
[16]T. S. Bush, J. D. Gale, C. R. A. Catlow, and P. D. Battle, J. Mater. Chem. **4**(6), 831–837 (1994).
[17]M. B. Sahariah and C. Y. Kadolkar, J. Phys.: Condens. Matter **19**(15), 156215 (2007).
[18]A. P. Bartók, M. C. Payne, R. Kondor, and G. Csányi, Phys. Rev. Lett. **104**(13), 136403 (2010).
[19]W. J. Szlachta, A. P. Bartók, and G. Csányi, Phys. Rev. B **90**(10), 104108 (2014).
[20]J. Behler and M. Parrinello, Phys. Rev. Lett. **98**(14), 146401 (2007).
[21]J. Behler, Phys. Chem. Chem. Phys. **13**(40), 17930–17955 (2011).
[22]A. P. Bartók, R. Kondor, and G. Csányi, Phys. Rev. B **87**(18), 184115 (2013).
[23]A. P. Thompson, L. P. Swiler, C. R. Trott, S. M. Foiles, and G. J. Tucker, J. Comput. Phys. **285**, 316–330 (2015).
[24]X. Li, C. Hu, C. Chen, Z. Deng, J. Luo, and S. P. Ong, Phys. Rev. B **98**(9), 094104 (2018).
[25]A. V. Shapeev, Multiscale Model. Simul. **14**(3), 1153–1173 (2016).
[26]E. V. Podryabinkin and A. V. Shapeev, Comput. Mater. Sci. **140**, 171–180 (2017).
[27]R. Drautz, Phys. Rev. B **99**(1), 014104 (2019).
[28]C. van der Oord, G. Csányi, and C. Ortner, Mach. Learn.: Sci. Technol. **1**(1), 015004 (2020).
[29]S. N. Pozdnyakov, M. J. Willatt, A. P. Bartók, C. Ortner, G. Csányi, and M. Ceriotti, arXiv:2001.11696 (2020).
[30]S. De, A. P. Bartók, G. Csányi, and M. Ceriotti, Phys. Chem. Chem. Phys. **18**(20), 13754–13769 (2016).
[31]A. P. Bartók, S. De, C. Poelking, N. Bernstein, J. R. Kermode, G. Csányi, and M. Ceriotti, Sci. Adv. **3**(12), e1701816 (2017).
[32]E. A. Engel, A. Anelli, M. Ceriotti, C. J. Pickard, and R. J. Needs, Nat. Commun. **9**(1), 2173 (2018).
[33]V. L. Deringer and G. Csányi, Phys. Rev. B **95**(9), 094203 (2017).
[34]V. L. Deringer, C. J. Pickard, and G. Csányi, Phys. Rev. Lett. **120**(15), 156001 (2018).
[35]J. Mavračić, F. C. Mocanu, V. L. Deringer, G. Csányi, and S. R. Elliott, J. Phys. Chem. Lett. **9**(11), 2985–2990 (2018).
[36]F. C. Mocanu, K. Konstantinou, T. H. Lee, N. Bernstein, V. L. Deringer, G. Csányi, and S. R. Elliott, J. Phys. Chem. B **122**(38), 8998–9006 (2018).
[37]P. Rowe, V. L. Deringer, P. Gasparotto, G. Csányi, and A. Michaelides, J. Chem. Phys. **153**(3), 034702 (2020).
[38]A. P. Bartók, J. Kermode, N. Bernstein, and G. Csányi, Phys. Rev. X **8**(4), 041048 (2018).
[39]Z. Zhang, G. Csányi, and D. Alfè, "Partitioning of sulfur between solid and liquid iron under Earth's core conditions: Constraints from atomistic simulations with machine learning potentials," Geochim. Cosmochim. Acta (published online 2020).
[40]M. Veit, S. K. Jain, S. Bonakala, I. Rudra, D. Hohl, and G. Csányi, J. Chem. Theory Comput. **15**(4), 2574–2586 (2019).
[41]T. T. Nguyen, E. Székely, G. Imbalzano, J. Behler, G. Csányi, M. Ceriotti, A. W. Götz, and F. Paesani, J. Chem. Phys. **148**(24), 241725 (2018).
[42]D. Dragoni, T. D. Daff, G. Csányi, and N. Marzari, Phys. Rev. Mater. **2**(1), 013808 (2018).
[43]C. E. Rasmussen and C. K. I. Williams, *Gaussian Processes for Machine Learning*, Adaptive Computation and Machine Learning (The MIT Press, 2005).
[44]Y. Liu, W. Hong, and B. Cao, Energy **188**, 116091 (2019).
[45]M. W. Mahoney and P. Drineas, Proc. Natl. Acad. Sci. U. S. A. **106**(3), 697 (2009).
[46]A. P. Bartók and G. Csányi, Int. J. Quantum Chem. **115**(16), 1051–1057 (2015).
[47]M. Ceriotti, M. J. Willatt, and G. Csányi, *Handbook of Materials Modeling: Methods, Theory and Modeling* (Springer International Publishing, Cham, 2018), pp. 1–27.
[48]G. Kresse and J. Furthmüller, Comput. Mater. Sci. **6**(1), 15–50 (1996).
[49]G. Kresse and D. Joubert, Phys. Rev. B **59**(3), 1758–1775 (1999).
[50]J. P. Perdew, K. Burke, and M. Ernzerhof, Phys. Rev. Lett. **77**(18), 3865–3868 (1996).
[51]P. E. Blöchl, Phys. Rev. B **50**(24), 17953–17979 (1994).
[52]J. Åhman, G. Svensson, and J. Albertsson, Acta Crystallogr., Sect. C: Cryst. Struct. Commun. **52**(6), 1336–1338 (1996).
[53]A. Togo, L. Chaput, I. Tanaka, and G. Hug, Phys. Rev. B **81**(17), 174301 (2010).
[54]Z. Guo, A. Verma, X. Wu, F. Sun, A. Hickman, T. Masui, A. Kuramata, M. Higashiwaki, D. Jena, and T. Luo, Appl. Phys. Lett. **106**(11), 111909 (2015).
[55]F. Orlandi, F. Mezzadri, G. Calestani, F. Boschi, and R. Fornari, Appl. Phys. Express **8**(11), 111101 (2015).
[56]S. Ghose, S. Rahman, L. Hong, J. S. Rojas-Ramirez, H. Jin, K. Park, R. Klie, and R. Droopad, J. Appl. Phys. **122**(9), 095302 (2017).
[57]A. Kalra, S. Vura, S. Rathkanthiwar, R. Muralidharan, S. Raghavan, and D. N. Nath, Appl. Phys. Express **11**(6), 064101 (2018).
[58]M. E. Liao, C. Li, H. M. Yu, E. Rosker, M. J. Tadjer, K. D. Hobart, and M. S. Goorsky, APL Mater. **7**(2), 022517 (2018).
[59]A. Togo and I. Tanaka, Scr. Mater. **108**, 1–5 (2015).
[60]W. Li, J. Carrete, N. A. Katcho, and N. Mingo, Comput. Phys. Commun. **185**(6), 1747–1758 (2014).
[61]P. Jiang, X. Qian, X. Li, and R. Yang, Appl. Phys. Lett. **113**(23), 232105 (2018).
[62]A. Carreras, A. Togo, and I. Tanaka, Comput. Phys. Commun. **221**, 221–234 (2017).
[63]T. Sun, D.-B. Zhang, and R. M. Wentzcovitch, Phys. Rev. B **89**(9), 094109 (2014).